This document is confidential and is proprietary to the American Chemical Society and its authors. Do not copy or disclose without written permission. If you have received this item in error, notify the sender and delete all copies.

Tuning the Electrocatalytic Oxygen Reduction Reaction Activity of PtCo Nanocrystals by Cobalt Concentration with Atomic-Scale Understanding

| Journal: | ACS Applied Materials & Interfaces |
|-------------------------------|---|
| Manuscript ID | am-2019-063467.R2 |
| Manuscript Type: | Article |
| Date Submitted by the Author: | 22-Jun-2019 |
| Complete List of Authors: | Lee, Jennifer; University of Pennsylvania, Chemistry Jishkariani, Davit; University of Pennsylvania, Chemistry Zhao, Yingrui; University of Pennsylvania, Materials Science and Engineering Najmr, Stan; University of Pennsylvania, Chemistry Rosen, Daniel; University of Pennsylvania, Materials Science and Engineering Kikkawa, James; University of Pennsylvania, Physics & Astronomy Stach, Eric; University of Pennsylvania School of Engineering and Applied Science, Engineering & Applied Science Murray, Christopher; University of Pennsylvania, |

SCHOLARONE™ Manuscripts

Tuning the Electrocatalytic Oxygen Reduction Reaction Activity of PtCo Nanocrystals by Cobalt Concentration with Atomic-Scale Understanding

Jennifer D. Lee,† Davit Jishkariani,†," Yingrui Zhao,‡ Stan Najmr,† Daniel Rosen,‡ James M. Kikkawa,§ Eric A. Stach,‡ Christopher B. Murray*,†,‡

†Department of Chemistry, University of Pennsylvania, Philadelphia, PA 19104, United States

[‡]Department of Materials Science and Engineering, University of Pennsylvania, Philadelphia, PA 19104, United States

§Department of Physics and Astronomy, University of Pennsylvania, Philadelphia, PA 19104, United States

KEYWORDS: nanocrystal electrocatalysis, platinum-cobalt alloy, structure-activity relationship, face-centered tetragonal structure, oxygen reduction reaction

ABSTRACT

The development of a suitable catalyst for the oxygen reduction reaction (ORR) – the cathode reaction of proton exchange membrane fuel cells (PEMFC) – is necessary to push this technology towards widespread adoption. There have been substantial efforts to utilize bimetallic Pt-M alloys that adopt the ordered face-centered tetragonal (L1₀) phase in order to reduce the usage of precious metal, enhance the ORR performance, and improve catalyst stability. In this work, monodisperse Pt-Co nanocrystals (NCs) with well-defined size (4-5 nm) and cobalt composition (25-75 at%) were synthesized via colloidal synthesis. The transformation from the chemically disordered A1 (face-centered cubic, fcc) to the L1₀ phase was achieved via thermal annealing using both a conventional oven and a rapid thermal annealing process. The structure of the Pt-Co catalysts was characterized by a variety of techniques, including transmission electron microscopy (TEM), energy dispersive X-ray spectroscopy in high-angle annular dark-field scanning transmission electron microscopy (STEM-EDS), small-angle X-ray scattering (SAXS), X-ray diffraction (XRD), and inductively coupled plasma-optical emission spectrometry (ICP-OES). The effects of annealing temperature on the composition-dependent degree of ordering, and subsequent effect on ORR activity is described. This work provides insights regarding the optimal spatial distribution of elements at the atomic level to achieve enhanced ORR activity and stability.

Introduction

Atomic-level understanding of catalytic performance has long been sought and may now be accessible through the use of combined techniques for characterizing the chemical, structural, and electronic properties *via* advanced microscopy and spectroscopy.^{1–7} However, heterogeneity in particle size, morphology, and composition often complicates efforts to identify the precise nature of the catalytically active sites.^{8–10} It is imperative to develop improved methods, both experimentally and theoretically, to accurately determine the factors that govern catalytic performance. Experimentally, it is essential to prepare as well-controlled materials as possible to help eliminate the contribution of structural heterogeneity in the interpretation of phenomena, and to help bridge the gap between single crystal, surface science studies, and the exploration of practical catalysts. The nanocrystals (NCs) produced *via* colloidal synthesis with controlled size, shape, and composition has achieved superior catalytic performance and stability in thermal catalysis,^{11–13} electrocatalysis,^{14–17} and photocatalysis.^{18,19} This, in turn, could enable a much deeper understanding of the catalytically related interface structures and the evolution of NC structure that results in superior catalytic performance.

One of the reactions that would benefit from atomic-scale understanding is the oxygen reduction reaction (ORR), which is the cathode reaction occurring in proton exchange membrane fuel cells (PEMFCs). PEMFCs are a critical technology to enhance the clean, sustainable production and usage of energy by converting hydrogen into electrical energy in automotive and portable applications. But practical realization of this technology is impeded by the high cost and low durability of the cathode catalysts that perform ORR.^{20–22} To date, extensive efforts have been devoted to introducing first-row transition metals (M) in Pt-M bimetallic nanoparticles as ORR catalysts to reduce the Pt loading and to modulate geometric, structural, and electronic effects in

order to improve ORR reaction rates.^{23–26} Other strategies include the formation of a monolayer Pt shell on the Pt-M alloy surface^{16,27–29} and the shape-controlled design of Pt-M alloys.^{16,30–32} These approaches have demonstrated significantly improved ORR activities. However, most Pt-M bimetallics reported to date are in the chemically disordered A1 phase (face-centered cubic, fcc) and are subject to instability due to uncontrolled leaching of the M component.^{20,24,33} To further improve catalyst stability, Pt-M (M=Fe, Co) alloys with a chemically ordered intermetallic structure, especially the L1₀-PtM phase (face-centered tetragonal, fct), have been considered to be one of the most promising materials.^{34–37} The L1₀ phase — in which Pt and M atoms alternate in layers along the c direction of the tetragonal cell — is well-studied for its hard-magnet properties^{38,39} and has also shown good stability in ORR reaction environments, especially in membrane electrode assembly (MEA) test conditions operated at 80 °C.^{36,37}

Among the bimetallic catalysts reported so far, Pt-Co systems have received considerable attention because of their relatively high ORR activities. They are currently one of the improved cathode catalysts that may replace pure Pt in commercial fuel cell vehicles.²⁴ In the exploration of the ordered intermetallic structure, most of the reports investigate NCs with the Pt₃Co composition, with the most active structure being a constrained Pt shell (2-3 atomic layers) with a Pt₃Co L1₂ ordered nanoparticle core.^{28,40} There are only limited reports regarding the performance of structurally ordered L1₀ intermetallic Pt-Co nanocatalysts for ORR reactions, and how Co composition contributes to the structural transformation process.^{36,41} Although correlations between Pt-Co alloy structure and ORR activity have been reported previously,^{42–44} due to the heterogeneity in alloy compositions and the presence of multiple phases in as-synthesized samples, a systematic correlation of structure-activity properties with a broad range of chemical compositions has not been reported to date.

Herein, we present the synthesis and characterization of a series of monodisperse Pt-Co bimetallic NCs with a series of compositions (Pt₃Co, PtCo, PtCo₂, and PtCo₃) that covers a large range of the Pt-Co compositions in the binary phase diagram. These NCs are supported on carbon, and have their ligands removed before being subjected to thermal treatment for structural conversion. The resulting Pt-Co samples are studied by a variety of techniques to identify changes in NC overall size and the structural ordering introduced by the conversion from the A1 to the L1₀ phase. The control over particle compositions achieved at the atomic scale allows us to establish a correlation between Co composition and the prominence of L1₀ phase. The degree of ordering is found to be closely related to the composition and further correlated with the ORR performance and catalyst stability. This study delineates how changes in crystal structure affect ORR performance *via* detailed quantitative analysis, which is the key to the design of bimetallic catalysts and the optimization of their catalytic performance.

Results and Discussion

Pt-Co NCs synthesis and characterization.

Monodisperse Pt-Co alloyed NCs with various compositions were synthesized by modifying a previously reported method^{13,45} *via* simultaneous reduction of platinum acetylacetonate (Pt(acac)₂) and thermal decomposition of dicobalt octacarbonyl (Co₂(CO)₈) in the presence of oleylamine (OLAM) and octadecene (Figure 1a-d). By changing the molar ratio of the Co and Pt precursors (Co₂(CO)₈, Pt(acac)₂) and the reaction time, the composition of Pt-Co NCs was readily tuned to be Pt₃Co, PtCo₂ and PtCo₃ (Supporting Information). All the elemental compositions referred in this report are determined by inductively coupled plasma-optical emission spectrometry (ICP-OES) measurements.

The as-prepared NCs are homogeneous in size, shape, and composition. The uniformity in size was confirmed by small-angle X-ray scattering (SAXS) data fitted to the Rayleigh function (Figure 1e) using Datasqueeze software. 46 The average particle sizes (diameter) and their distributions are summarized in Table S1. The NCs exhibit monodispersity with sizes ranging from 4.6 to 5.8 nm and standard deviations less than 20%. The transmission electron microscopy (TEM) images of Pt-Co alloys in Figure 1a-d indicate that the particles are uniform and spherical in shape, in good agreement with previous studies.¹³ The X-ray diffraction (XRD) patterns of Pt-Co NCs with different compositions shown in Figure 1f indicate the presence of the chemically disordered A1 phase, with two diffraction peaks at 40.0° and 46.9° corresponding to the (111) and (200) planes respectively. ¹³ The shifts of the reflections to higher angles in 2θ with increasing Co concentration, relative to monometallic Pt, indicates the incorporation of Co into the Pt fcc structure to form an alloy phase with a lattice contraction consistent with Vegard's law (Figure S1). X-ray scattering simulations were utilized to calculate the scattering patterns and extract the crystalline Pt-Co structures. The XRD data in Figure 1f were fitted with the atomistic simulation of X-ray scattering based on the Debye equation.⁴⁷ The Co atomic % (at %) that contributes to the fcc crystallographic registry directly correlated with the Co at % obtained from ICP-OES results.

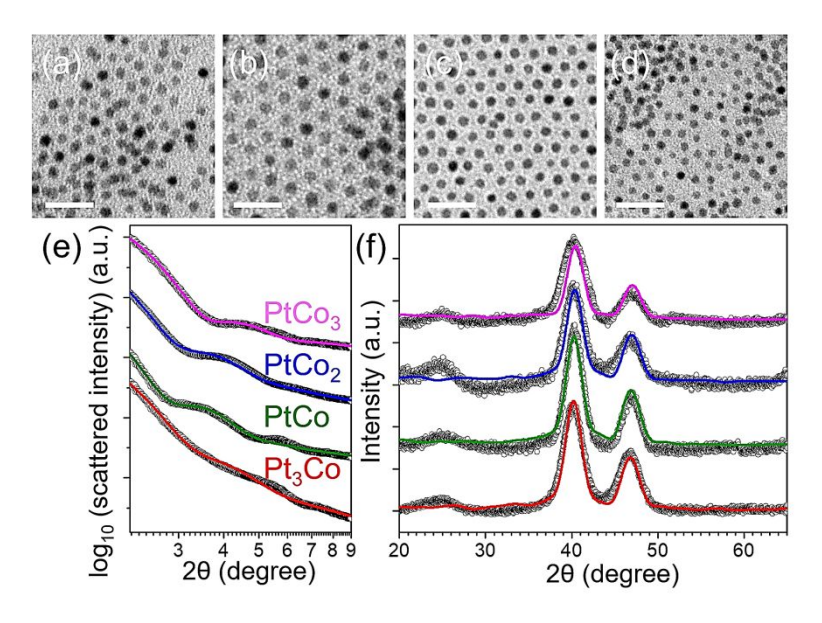


Figure 1. TEM images of as-synthesized (a) Pt₃Co, (b) PtCo₂ (c) PtCo₂ and (d) PtCo₃ NCs, the corresponding (e) SAXS and (f) XRD patterns. The black circles in (e) and (f) represent the observed data. The solid lines in (e) and (f) represent the simulated fits for the size and crystal structure, respectively. Scale bars in (a)-(d) are 20 nm.

The as-synthesized NCs were dispersed onto carbon support to prepare 20 wt% of metals on carbon (Pt-Co/C). The three-dimensional (3D) spatial distribution of NCs on carbon was visualized by electron tomography. A bright-field image of Pt₃Co/C is shown in Figure 2a and the corresponding 3D reconstructed tomogram is shown in Figure 2b (see a 3D rotation of the tomogram in Supporting Information Movie 1). The high Z-coefficient of Pt and Co versus C allows for contrast-based 3D elemental mapping of these structures. These data highlight that the NCs are well-dispersed onto the carbon support after deposition, which would minimize the aggregation caused by thermal treatment carried out later in the process. To remove the surface organic ligands surrounding NCs, a two-step ligand removal process, which involves first exposing to oxygen plasma followed by thermal annealing at 500 °C, was carried out (Supporting Information), which has shown efficient ligand removal with no effect on the size, morphology and crystal structure of

NCs.⁴⁸ To show the control over particle composition at the atomic scale, the composition of Pt₃Co/C was probed with energy dispersive X-ray spectroscopy (EDS) in high-angle annular dark-field scanning transmission electron microscopy (STEM-HAADF) and compared with results obtained from ICP-OES (Figure 2c-h). ICP-OES determines the bulk at % of Pt and Co but does not provide sufficient information on the composition distribution within a single particle. To probe the uniformity of Pt and Co at the single-particle level, STEM-EDS elemental mapping allows statistical analysis of composition distributions of individual particles. From the presented STEM-EDS maps (Figure 2c-f), the atomic percentage (at %) of Pt and Co in 15 individual particles was analyzed with the Pt at % ranging from 71 to 90 at % (Figure 2g). The average Pt:Co ratios over 15 particles was in good agreement with the ensemble average obtained from ICP-OES (Figure 2h), and the results presented here are representative over the entire sample. This synthetic method allows good control over particle composition with homogeneity achieved at the atomic scale. This degree of control allows the direct correlation of the bimetallic NC compositions to structure ordering and electrochemical activity.

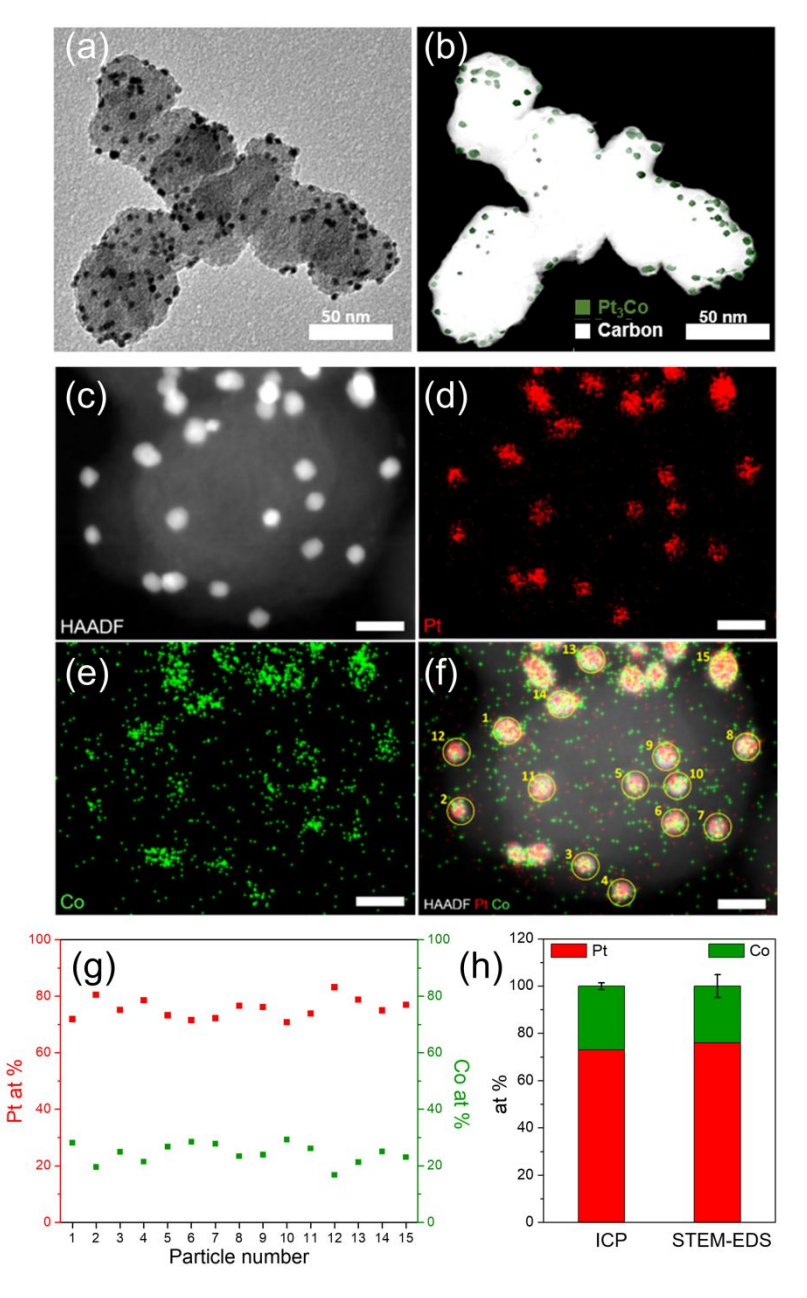


Figure 2. (a) Bright-field TEM image of Pt₃Co/C and (b) the corresponding single image taken from the 3D tomographic reconstruction (also see Supporting Information Movie 1). (c) STEM-HAADF and EDS elemental mapping from a different sample area of (d) Pt, (e) Co and (f) overlay of Pt₃Co/C NCs. (g) Composition of individual particles analyzed from (f). (h) Comparison of Pt and Co at % measured by different methods. Scale bars in (c)-(f) are 10 nm. Numbering in (f) corresponds to the particle numbers in (g).

Structural analysis of thermally-treated Pt-Co/C.

A thermal annealing process is required to convert the disordered A1 phase into the chemically ordered L1₀ phase. The Pt-Co/C was converted by heating under a flow of 5% H₂ (balanced by Ar) in a tube furnace. To identify the lowest temperature for the phase transformation to occur, PtCo₂/C was heated at different temperatures and times. Figure S2 shows the series of diffraction patterns resulting from these treatments. In comparison with the as-synthesized PtCo₂/C, thermal annealing at 550 °C for 2 h did seem to result in an early stage of ordering in the crystal structure, as indicated by the shifts of the reflections to higher angles in 20, however, no extra diffraction peak was observed until the annealing temperature exceeded 650 °C. At this point, the extra peak at 33.3° can be indexed as the 110 reflections of the L1₀ phase [PDF no. 97-010-2622]. The 110 reflections of the L1₀ phase at 24° partially overlap with the graphite 002 peak from the Vulcan carbon supports at ~25°. 48 For temperatures higher than 650 °C, the atomic diffusion inside the NCs is fast enough to drive the transformation to the L1₀ phase; however, extended thermal treatment would introduce phase segregation of pure Pt [PDF no. 04-0802] from the L1₀ phase in the sample. This is evident from the splitting of peaks that correspond to the (111) and (200) planes in the XRD pattern of PtCo₂/C treated at 800 °C for 8 h.⁴⁹

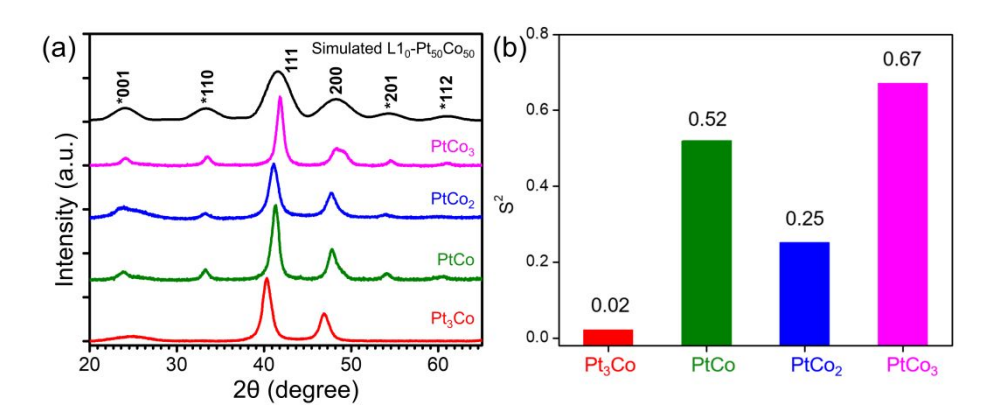


Figure 3. (a) The XRD patterns of carbon-supported Pt₃Co (red), PtCo (green), PtCo₂ (blue) and PtCo₃ (magenta) after 650 °C / 4 h of thermal treatment. The black line represents the X-ray

scattering simulation results of $L1_0$ -Pt₅₀Co₅₀. (b) Dependence of the degree of ordering (S²) and for different Co compositions. The degree of ordering is calculated from the XRD patterns in (a). Peaks labeled with an asterisk in (a) correspond to the $L1_0$ phase.

Thus, thermal annealing at 650 °C for 4 h under 5% H₂ (balanced by Ar) was chosen as the condition to convert samples with different Co compositions to the L1₀ phase. The advantage of starting with smaller size particles was clear as the inevitable particle size increase during high-temperature treatment yielded the final sizes within 6-10 nm range that is well regarded as a critical size range for Pt-M bimetallic systems for improved ORR performance and avoiding nanoporosity. The TEM images provided in Figure S3 indicate such change in particle size where the average sizes changed from 4.6-5.8 nm to 6.0-9.7 nm and standard deviation changed from less than 20% to 34%. The sizes calculated from SAXS data fitted to the Rayleigh function (Figure S4) were in good agreement with the crystal domain sizes estimated using the line broadening of the XRD patterns with the Debye–Scherrer equation (Table S2).^{50,51}

The presence of the 110 superstructure peak in the XRD patterns of thermally-treated Pt-Co/C (Figure 3a and S5) indicates all four compositions are converted into the L1₀ phase. X-ray simulations were performed to provide the XRD pattern of a perfectly ordered L1₀ phase.⁴⁷ The simulation generated from the Debye equation was based on the construction of an atomistic model of a 5 nm L1₀-Pt₅₀Co₅₀ (50 at wt% Pt) nanoparticle with Space Group P4/mmm and lattice parameters a/c = 2.682/3.675 (Å/Å).⁴⁴ Quantitative analysis of the phase transformation from the A1 to the L1₀ phase is presented as a "degree of ordering", with an order parameter S² introduced as described below.⁵² From the XRD patterns, we determined the integrated intensity ratios, I_{110}/I_{111} , and extracted the degree of long-range chemical ordering, S², defined in Equation (1) as the probability of correct site occupation in the L1₀ lattice:

$$S^{2} = \frac{\left\{I_{110}/I_{111}\right\}_{measured}}{\left\{I_{110}/I_{111}\right\}_{S=1}} \tag{1}$$

where $\{I_{110}/I_{111}\}_{measured}$ and $\{I_{110}/I_{111}\}_{S=1}$ are the integrated intensity ratio of 001/111 peaks for the measured sample and the simulated perfect L1₀ phase, respectively.^{52,53} The relationship between S² and Co composition is shown in Figure 3b. Figure 3b suggests that the increase in Co concentration can promote the process of chemical ordering. This is especially true for the samples with a 1:1 Pt:Co ratio, where the phase diagram for the Pt-Co binary system indicates that the L1₀ phase is the equilibrium phase.⁵⁴ It was found that over 50% conversion of A1 to L1₀ phase was achieved. Similar composition-dependency of S² was also observed when an alternative thermal treatment was applied to the Pt-Co/C. A rapid thermal annealing (RTA) process with a heating rate of up to 200 °C/s has been used to introduce chemical ordering in PtFe nanoparticles with a lower annealing temperature and shorter time.⁵⁵ During the course of this research, the phase transformation of Pt-Co/C samples were investigated with both an RTA process (Figure S6) and the use of a tube furnace (Figure 3). While both of these methods achieved reasonable S², those treated in the tube furnace had the highest degree of ordering (Figure 3b).

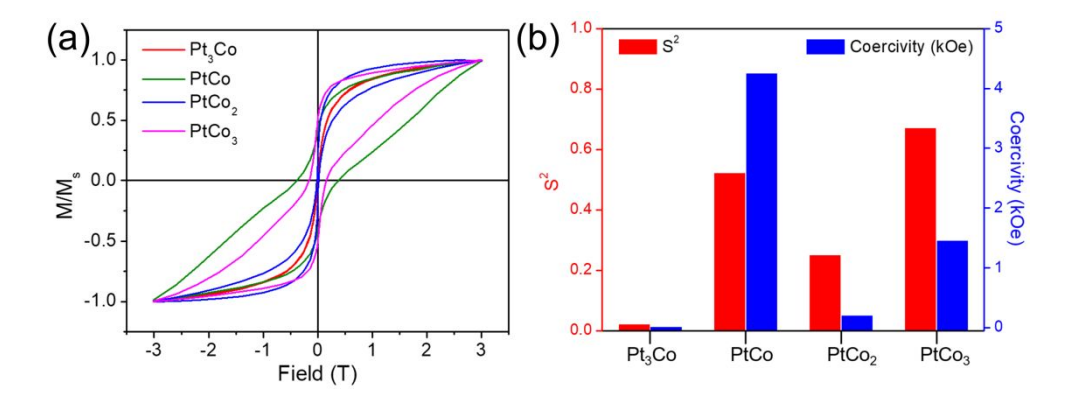


Figure 4. (a) Hysteresis curves at 300 K of carbon-supported Pt₃Co (red), PtCo (green), PtCo₂ (blue) and PtCo₃ (magenta) after 650 °C / 4 h of thermal treatment and the corresponding (b) degree of ordering (S²) and coercivity (H_c).

Thermally-treated PtCo₃/C showed the highest degree of ordering, assuming the structure is converted to the L1₀ phase. However, based on the phase diagram of Pt-Co binary system, ⁵⁴ with Co concentration higher than 60%, there is the possible existence of a third phase: the hexagonal close-packed (hcp) phase. To determine if that the calculated S² of PtCo₃ is a result of contributions from both the L1₀ and hcp phase, direct current (DC) magnetic characterization with SQUID magnetometry was applied to probe the existence of the hcp phase. The transition of magnetic behavior from superparamagnetic to ferromagnetic is a typical indicator for the presence of the L₁₀ phase, because the L₁₀ phase is strongly ferromagnetic at room temperature, while the A₁ phase is superparamagnetic with no coercivity (H_c) . ^{36,38} From the hysteresis curves measured at 300 K of the as-prepared PtCo/C and PtCo₃/C samples (Figure S7), the H_c are 0.03 and 0.05 kOe, respectively. The existence of close-to-zero values in H_c is the typical feature of superparamagnetism.³⁸ The hysteresis loops at 300 K shown in Figure 4a for thermally-treated Pt-Co/C samples exhibit two-phase behaviors, indicating the presence of mixed soft and hard magnet behaviors. The presence of the $L1_0$ phase would be reflected in the increase in H_c , because the tetragonal symmetry exhibits high magnetocrystalline anisotropy (K_u) with the short c axis being the easy axis of magnetization. 36,38 The H_c of thermally-treated PtCo/C and PtCo₃/C are 4.25 and 1.45 kOe, respectively, which is in good agreement with the XRD results of the existence of L1₀ phase (Figure 4b). We calculate the K_u values of thermally-treated Pt-Co/C samples based on H_c = $2K_u/M_s$, using H_c and M_s extracted from the hysteresis curves measured at 15 K.⁵⁶ The result (Figure S8) correlates well with the degree of ordering shown in Figure 4b. Furthermore, the

higher H_c of thermally-treated PtCo/C compared to PtCo₃/C indicates the presence of a relatively lower L1₀ phase in PtCo₃/C. Although the hcp phase also has a ferromagnetic behavior, a 2 times smaller K_u of 2.0×10^7 erg/cm³ in hcp PtCo₃, compared to 4.9×10^7 erg/cm³ in L1₀ phase PtCo has been reported for bulk materials.⁵⁷ Based on the XRD and DC magnetic characterization data, the L1₀ phase formation can be strongly influenced by varying the concentration of Co in the system with PtCo/C showing the highest degree of ordering of the L1₀ phase.

Electrochemical study of thermally-treated Pt-Co/C.

To understand the relation between the degree of ordering and the ORR performance, the ORR activity of the thermally-treated Pt-Co/C catalysts was determined. The catalysts were dispersed in a mixture of isopropanol, water, and Nafion® using sonication. The catalyst ink was transferred onto a 6 mm glassy carbon surface of a rotating disk electrode (RDE), forming an electrode decorated by a thin film of catalysts. Commercial Pt/C (comm-Pt/C, Fuel Cell Store, 2.0-3.0 nm Pt with 20% mass loading on Vulcan XC-72 carbon support) catalyst ink was prepared using the same procedure to provide a benchmark catalyst. The cyclic voltammograms (CV) in Figure S9 of four thermally-treated Pt-Co/C catalysts all showed the typical hydrogen underpotential formation/stripping peaks as expected for comm-Pt/C.58 The electrodes were pre-treated by cycling the potential for 100 cycles to remove surface contamination before further testing. The electrochemically active surface areas (ECSAs) were estimated by the integrated areas between 0.05 and 0.4 V vs RHE (Table S3).⁵⁸ The compositions with the larger average particle sizes (PtCo/C, PtCo₃/C) showed higher ECSAs compared to the compositions with the smaller average particle sizes (Pt₃Co/C, PtCo₂/C). This is likely due to a combination of multiple factors, including the degree of ordering, 41 Pt segregation at the near surface region under thermal treatment, 28 and

the formation of thin Pt skin as a result of electrochemical dealloying,⁵⁹ and cannot be explained by the particle size difference alone.

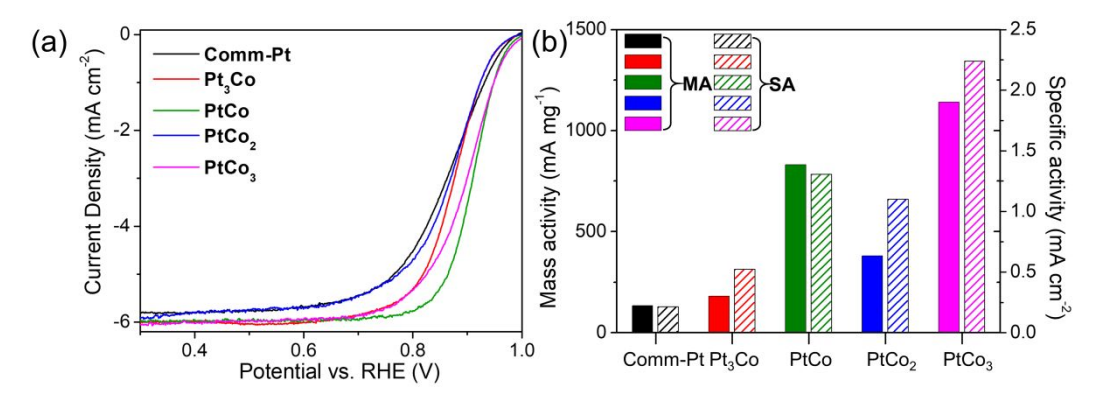


Figure 5. (a) ORR polarization curves and (b) mass and specific activities at 0.9V (vs RHE) of the commercial Pt/C, thermally-treated Pt₃Co/C, PtCo₂/C, PtCo₂/C, and PtCo₃/C catalysts.

The polarization curves (Figure 5a) for the ORR were obtained with thermally-treated Pt-Co/C catalysts in an O_2 -saturated 0.1M HClO₄ solution, at room temperature, with the rotation rate of 1600 rpm and the sweep rate of 10 mV s⁻¹ and the corresponding Tafel plot is shown in Figure S10. At high potentials (> 0.9 V vs RHE), the Tafel slope of comm-Pt is about -70 mV/decade, which is in agreement with previous reports. 16,36 For all thermally-treated Pt-Co/C catalysts, the Tafel slopes are between -56–65 mV/decade, indicating improved ORR kinetics compared to comm-Pt. 16,36 To better evaluate these NCs, we extracted specific activity (SA) and mass activity (MA) values that can be used to evaluate their ORR activity. An absolute activity comparison of thermally-treated Pt-Co/C with comm-Pt/C is shown in Figure 5b. The SA and MA were extracted by normalizing their ORR kinetic current (I_k) at 0.9V vs RHE over ECSA and the amount of Pt, respectively. The kinetic current can be calculated using the Koutechy-Levich equation. 60 The SA and MA of comm-Pt/C reported here coincide well with previous RDE studies. 36 The results correlate well with the degree of ordering shown in Figure 3b. Because there is a lower cobalt

composition in Pt₃Co/C, the low degree of ordering suggests an unsuccessful phase transformation and that the catalyst remained in the A1 phase, which resulted in low ORR activities. With increasing Co concentration and degree of ordering, the catalysts exhibit superior ORR activities compared to comm-Pt/C. It has been shown that the presence of Co facilitates ORR reaction kinetics, particularly in the reduction steps involving Pt-O bond breaking, which contributes to the superior performance of Pt-M alloys.⁴ Increased ORR activity has also been attributed to the presence of fct-PtCo and fcc-PtCo phases.61 To better compare the ORR activity between thermally-treated Pt-Co/C catalysts, improvement factors of MA and SA of PtCo/C, PtCo₂/C and PtCo₃/C are calculated against Pt₃Co/C (Figure S11). When MA and SA improvement factors are plotted against particle size (Figure S11a) and S² (Figure S11b), the stronger correlation between enhanced ORR activity and degree of ordering as opposed to change in particle size is observed. Comparing thermally-treated PtCo₂/C to Pt₃Co/C, which showed similar sizes of 6.3±1.5 and 6.0±1.6 nm, respectively, an activity improvement factor of 2.1 in SA is observed in PtCo₂/C. A similar phenomenon is also observed when comparing PtCo/C with PtCo₃/C. This is a clear indication that the demonstrated enhancement in intrinsic SA arises from the L1₀ structure. It is also known that increasing particle size would lead to a decrease in MA due to decreased surface area. 62,63 However, in our study, both PtCo/C and PtCo₃/C with larger particle sizes compared to Pt₃Co/C showed increased MA activity improvement factor of 4.6 and 6.3, respectively. Therefore, the improvement trend in MA and SA correlates better with the degree of ordering (S²) and is less affected by the particle size within the size range tested. This correlation is further established here with a quantitative analysis of the composition-dependent degree of ordering, which was inaccessible in previous studies due to heterogeneity in as-prepared samples.

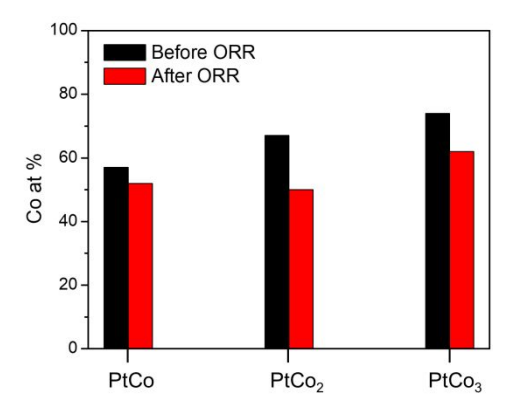


Figure 6. Co at % of thermally-treated PtCo/C, PtCo₂/C and PtCo₃/C measured by ICP-OES before and after the ORR testing.

The thermally-treated PtCo₃/C showed the highest ORR activity among the four Pt-Co compositions, however, the Co-rich catalyst was observed to be the most vulnerable to corrosion during the electrochemical measurements. 43,64 The stability of the catalysts was evaluated by the leaching of cobalt composition after the ORR testing. The elemental compositions were quantitatively determined by ICP-OES measurements of catalysts before and after the electrochemical testing (Figure 6). The results indicated that the Co at% is reduced after the electrochemical testing and a reduction of 8%, 25%, and 16% is observed for PtCo/C, PtCo₂/C, and PtCo₃/C, respectively. Taking into account both ORR activity and catalyst stability, PtCo/C resulted in the best performance: it not only outperforms the comm-Pt/C but also Pt₃Co/C, which is the most widely reported bimetallic composition. 42,64 The PtCo/C also showed the highest stability, with only 8% of Co leaching after the ORR testing. We also investigated the PtCo/C stability by cycling in the potential range of 0.6 to 1.0 V vs RHE in O₂-saturated 0.1 M HClO₄. After 5000 cycles, we observe no change in Co at% and only 21% of Co leaching after 25,000 cycles (Figure S12). The stability of PtCo/C is also confirmed with TEM images and CV curves collected at the beginning of life (BOL) and after 5000 and 25,000 potential scans (Figure S13). A 32% drop in ECSA after 5000 cycles was observed and maintained at a stable level after 25,000

cycles with no obvious change observed in TEM images. The comm-Pt/C shows a 61% drop in ECSA after 25,000 cycles with TEM images showing the obvious size growth and aggregation of NPs during stability test. This result suggests that higher ORR performance can be achieved by reducing the amount of Pt up to 50%.

A systematic set of Pt-Co with compositions covering a wide range of the phase diagram of Pt-Co binary system were synthesized with homogeneity in size, shape, and composition. This is confirmed by the quantitative analyses of TEM, SAXS, STEM-EDS, and ICP-OES results. This degree of control allows us to establish an atomic understanding of the correlation between Co compositions and the structural ordering introduced by the thermal transformation from the A1 to the L1₀ phase. The structural ordering (S²) was quantified by XRD analysis and showed a strong dependency on the annealing temperatures and Co compositions. The increase in Co concentration promotes the process of chemical ordering and over 50% conversion was shown with thermally-treated PtCo/C. Further correlations were observed between XRD analysis and magnetic properties to characterize the structural ordering. The combination of techniques helps to clarify the contribution from multiple phases in thermally-treated PtCo₃/C. The detailed understanding in Pt-Co compositions and crystal structures helps to establish structure-property relations in crystal structures and ORR performance with the best ORR catalyst identified as the thermally-treated PtCo/C catalysts with consideration of both activity and stability in acidic condition.

Conclusion

In summary, this work presents a detailed understanding of the contribution of Co composition to structural changes and ORR activities of Pt-Co alloys. Monodisperse Pt-Co nanocrystals (NCs) were synthesized with atomic-scale homogeneity in size (4-5 nm) and cobalt composition (25-75 at%) and characterized with various techniques, including TEM, STEM-EDS, SAXS, XRD, and

ICP-OES. The successful thermal transformation from the A1 to the L1₀ phase was demonstrated with quantification of the degree of ordering based on XRD and DC magnetic data. The composition-dependent degree of ordering was found to correlate with the ORR activity and thermally-treated PtCo/C showed the best performance in terms of ORR activity and stability in an acidic environment. This work provides fundamental insights into the intrinsic correlation between the relevant ORR activity enhancement, the chemical compositions of Pt-Co alloy catalysts and the ordering structures, and thus aids research efforts towards developing the best possible catalytic materials for fuel cell applications.

ASSOCIATED CONTENT

Supporting Information. Figure S1-S13 Tables S1-S3, Movie 1 and movie caption and details of experimental methods are available. This material is available free of charge *via* the Internet at http://pubs.acs.org.

AUTHOR INFORMATION

Corresponding Author

*E-mail: cbmurray@sas.upenn.edu

Present Addresses

"Chemical and Nanoparticle Synthesis Core, University of Pennsylvania, Philadelphia, PA 19104, United States

Author Contributions

All authors have given approval to the final version of the manuscript.

Notes

The authors declare no competing financial interest.

ACKNOWLEDGMENT

The work was supported by the US Department of Energy, Energy Efficiency and Renewable Energy, Fuel Cell Technology Office. Los Alamos National Laboratory is operated by Los Alamos National Security, LLC under Contract DE-AC52-06NA25396. This research used resources of the Center for Functional Nanomaterials, Brookhaven National Laboratory (BNL), and was supported by the U.S. Department of Energy, Office of Science, Office of Workforce Development for Teachers and Scientists, Office of Science Graduate Student Research (SCGSR) program. J.D.L acknowledge the support from the SCGSR program, which is administered by the Oak Ridge Institute for Science and Education (ORISE) for the DOE. ORISE is managed by ORAU under contract number DE-SC0014664. Magnetic property measurements were supported by NSF MRSEC DMR-1720530. J.D.L acknowledges Dr. Kotaro Sasaki at the Brookhaven National Laboratory for the assistance with the RDE measurements at the Chemistry Division. C.B.M. acknowledges the Richard Perry University Professorship at the University of Pennsylvania.

REFERENCES

(1) Wang, D.; Liu, S.; Wang, J.; Lin, R.; Kawasaki, M.; Rus, E.; Silberstein, K. E.; Lowe, M. A.; Lin, F.; Nordlund, D.; Lui, H.; Muller, D. A.; Xin, H. L.; Abruña, H. D. Spontaneous Incorporation of Gold in Palladium-Based Ternary Nanoparticles Makes Durable Electrocatalysts for Oxygen Reduction Reaction. *Nat. Commun.* **2016**, 7, 1–9.

- (2) Meier, J. C.; Galeano, C.; Katsounaros, I.; Topalov, A. A.; Kostka, A.; Schüth, F.; Mayrhofer, K. J. J. Degradation Mechanisms of Pt/C Fuel Cell Catalysts under Simulated Start-Stop Conditions. *ACS Catal.* **2012**, 2, 832–843.
- (3) Li, Y.; Zakharov, D.; Zhao, S.; Tappero, R.; Jung, U.; Elsen, A.; Baumann, P.; Nuzzo, R. G.; Stach, E. A.; Frenkel, A. I. Complex Structural Dynamics of Nanocatalysts Revealed in Operando Conditions by Correlated Imaging and Spectroscopy Probes. *Nat. Commun.* **2015**, 6, 1–6.
- (4) Ishiguro, N.; Saida, T.; Uruga, T.; Nagamatsu, S.; Sekizawa, O.; Nitta, K.; Yamamoto, T.; Ohkoshi, S.; Iwasawa, Y.; Yokoyama, T.; Tada, M. Operando Time-Resolved X-Ray Absorption Fine Structure Study for Surface Events on a Pt₃Co/C Cathode Catalyst in a Polymer Electrolyte Fuel Cell during Voltage-Operating Processes. *ACS Catal.* **2012**, 2, 1319–1330.
- (5) Zugic, B.; Wang, L.; Heine, C.; Zakharov, D. N.; Lechner, B. A. J.; Stach, E. A.; Biener, J.; Salmeron, M.; Madix, R. J.; Friend, C. M. Dynamic Restructuring Drives Catalytic Activity on Nanoporous Gold-Silver Alloy Catalysts. *Nat. Mater.* **2017**, 16, 558–564.
- (6) Liu, D.; Li, Y.; Kottwitz, M.; Yan, B.; Yao, S.; Gamalski, A.; Grolimund, D.; Safonova, O. V.; Nachtegaal, M.; Chen, J. G.; Stach, E. A.; Nuzzo, R. G.; Frenkel, A. I. Identifying Dynamic Structural Changes of Active Sites in Pt–Ni Bimetallic Catalysts Using Multimodal Approaches. *ACS Catal.* **2018**, 8, 4120–4131.
- (7) Goulas, K. A.; Lee, J. D.; Zheng, W.; Lym, J.; Yao, S.; Oh, D. S.; Wang, C.; Gorte, R. J.; Chen, J. G.; Murray, C. B.; Vlachos, D. G. Spectroscopic Characterization of a Highly Selective NiCu₃/C Hydrodeoxygenation Catalyst. *Catal. Sci. Technol.* **2018**, 8, 6100–6108.

- (8) Beermann, V.; Gocyla, M.; Kühl, S.; Padgett, E.; Schmies, H.; Goerlin, M.; Erini, N.; Shviro, M.; Heggen, M.; Dunin-Borkowski, R. E.; Muller, D. A.; Strasser, P. Tuning the Electrocatalytic Oxygen Reduction Reaction Activity and Stability of Shape-Controlled Pt–Ni Nanoparticles by Thermal Annealing Elucidating the Surface Atomic Structural and Compositional Changes. *J. Am. Chem. Soc.* **2017**, 139, 16536–16547.
- (9) Han, L.; Meng, Q.; Wang, D.; Zhu, Y.; Wang, J.; Du, X.; Stach, E. A.; Xin, H. L. Interrogation of Bimetallic Particle Oxidation in Three Dimensions at the Nanoscale. *Nat. Commun.* **2016**, 7, 1–9.
- (10) Wang, G.-H.; Hilgert, J.; Richter, F. H.; Wang, F.; Bongard, H.-J.; Spliethoff, B.; Weidenthaler, C.; Schüth, F. Platinum-Cobalt Bimetallic Nanoparticles in Hollow Carbon Nanospheres for Hydrogenolysis of 5-Hydroxymethylfurfural. *Nat. Mater.* **2014**, 13, 293–300.
- (11) Cargnello, M. Colloidal Nanocrystals as Building Blocks for Well-De Fi Ned Heterogeneous Catalysts. *Chem. Mater.* **2019**, 31, 576–596.
- (12) Cargnello, M.; Doan-Nguyen, V. V. T.; Gordon, T. R.; Diaz, R. E.; Stach, E. A.; Gorte, R. J.; Fornasiero, P.; Murray, C. B. Control of Metal Nanocrystal Size Reveals Metal-Support Interface Role for Ceria Catalysts. *Science* **2013**, 341, 771–773.
- (13) Luo, J.; Yun, H.; Mironenko, A. V.; Goulas, K.; Lee, J. D.; Monai, M.; Wang, C.; Vorotnikov, V.; Murray, C. B.; Vlachos, D. G.; Fornasiero, P.; Gorte, R. J. Mechanisms for High Selectivity in the Hydrodeoxygenation of 5-Hydroxymethylfurfural over PtCo Nanocrystals. *ACS Catal.* **2016**, 6, 4095–4104.

- (14) Guo, S.; Zhang, S.; Sun, S. Tuning Nanoparticle Catalysis for the Oxygen Reduction Reaction. *Angew. Chem.*, *Int. Ed.* **2013**, 52, 8526–8544.
- (15) Wang, C.; Markovic, N. M.; Stamenkovic, V. R. Advanced Platinum Alloy Electrocatalysts for the Oxygen Reduction Reaction. *ACS Catal.* **2012**, 2, 891–898.
- (16) Chen, C.; Kang, Y.; Huo, Z.; Zhu, Z.; Huang, W.; Xin, H. L.; Snyder, J. D.; Li, D.; Herron, J. A.; Mavrikakis, M.; Chi, M.; More, K. L.; Li, Y.; Markovic, N. M.; Somorjai, G. A.; Yang, P. Highly Crystalline Multimetallic Nanoframes with Three-Dimensional Electrocatalytic Surfaces. *Science* **2014**, *343*, 1339–1343.
- (17) Zhang, S.; Hao, Y.; Su, D.; Doan-nguyen, V. V. T.; Wu, Y.; Li, J.; Sun, S.; Murray, C. B. Monodisperse Core/Shell Ni/FePt Nanoparticles and Their Conversion to Ni/Pt to Catalyze Oxygen Reduction. *J. Am. Chem. Soc.* **2014**, 136, 8–11.
- (18) Gordon, T. R.; Cargnello, M.; Paik, T.; Mangolini, F.; Weber, R. T.; Fornasiero, P.; Murray, C. B. Nonaqueous Synthesis of TiO₂ Nanocrystals Using TiF₄ to Engineer Morphology, Oxygen Vacancy Concentration, and Photocatalytic Activity. *J. Am. Chem. Soc.* **2012**, 134, 6751–6761.
- (19) Pepin, P. A.; Lee, J. D.; Murray, C. B.; Vohs, J. M. Thermal and Photocatalytic Reactions of Methanol and Acetaldehyde on Pt-Modified Brookite TiO₂ Nanorods. *ACS Catal.* **2018**, 8, 11834–11846.
- (20) Stephens, I. E. L.; Rossmeisl, J.; Chorkendorff, I. Toward Sustainable Fuel Cells. *Science* **2016**, 354, 1378–1379.

- (21) Debe, M. K. Electrocatalyst Approaches and Challenges for Automotive Fuel Cells. *Nature* **2012**, 486, 43–51.
- (22) Kongkanand, A.; Mathias, M. F. The Priority and Challenge of High-Power Performance of Low-Platinum Proton-Exchange Membrane Fuel Cells. *J. Phys. Chem. Lett.* **2016**, 7, 1127–1137.
- (23) Luo, M.; Guo, S. Strain-Controlled Electrocatalysis on Multimetallic Nanomaterials. *Nat. Rev. Mater.* **2017**, 2, 1–14.
- (24) Stamenkovic, V. R.; Mun, B. S.; Arenz, M.; Mayrhofer, K. J. J.; Lucas, C. A.; Wang, G.; Ross, P. N.; Markovic, N. M. Trends in Electrocatalysis on Extended and Nanoscale Pt-Bimetallic Alloy Surfaces. *Nat. Mater.* **2007**, 6, 241–247.
- (25) Scofield, M. E.; Liu, H.; Wong, S. S. A Concise Guide to Sustainable PEMFCs: Recent Advances in Improving both Oxygen Reduction Catalysts and Proton Exchange Membranes. *Chem. Soc. Rev.* **2015**, 44, 5836–5860.
- (26) Shao, M.; Chang, Q.; Dodelet, J.-P.; Chenitz, R. Recent Advances in Electrocatalysts for Oxygen Reduction Reaction. *Chem. Rev.* **2016**, 116, 3594–3657.
- (27) Sasaki, K.; Naohara, H.; Cai, Y.; Choi, Y. M.; Liu, P.; Vukmirovic, M. B.; Wang, J. X.; Adzic, R. R. Communications Core-Protected Platinum Monolayer Shell High-Stability Electrocatalysts for Fuel-Cell Cathodes. *Angew. Chem. Int. Ed.* **2010**, 49, 8602–8607.
- (28) Wang, D.; Xin, H. L.; Hovden, R.; Wang, H.; Yu, Y.; Muller, D. A.; Disalvo, F. J.; Abruña, H. D. Structurally Ordered Intermetallic Platinum-Cobalt Core-Shell Nanoparticles with Enhanced Activity and Stability as Oxygen Reduction Electrocatalysts. *Nat. Mater.* **2013**, 12, 81–87.

- (29) Stamenkovic, V. R.; Mun, B. S.; Mayrhofer, K. J. J.; Ross, P. N.; Markovic, N. M. Effect of Surface Composition on Electronic Structure, Stability, and Electrocatalytic Properties of Pt-Transition Metal Alloys: Pt-Skin versus Pt-Skeleton Surfaces. *J. Am. Chem. Soc.* **2006**, 128, 8813–8819.
- (30) Cui, C.; Gan, L.; Heggen, M.; Rudi, S.; Strasser, P. Compositional Segregation in Shaped Pt Alloy Nanoparticles and Their Structural Behaviour during Electrocatalysis. *Nat. Mater.* **2013**, 12, 765–771.
- (31) Huang, X.; Zhao, Z.; Cao, L.; Chen, Y.; Zhu, E.; Lin, Z.; Li, M.; Yan, A.; Zettl, A.; Wang, Y. M.; Duan, X.; Mueller, T.; Huang, Y. High-Performance Transition Metal-doped Pt₃Ni Octahedra for Oxygen Reduction Reaction. *Science* **2015**, 348, 1230–1234.
- (32) Stamenkovic, V. R.; Fowler, B.; Mun, B. S.; Wang, G.; Ross, P. N.; Lucas, C. A.; Marković, N. M. Improved Oxygen Reduction Activity on Pt₃Ni(111) via Increased Surface Site Availability. *Science* **2007**, 315, 493–497.
- (33) Xin, H. L.; Alayoglu, S.; Tao, R.; Genc, A.; Wang, C.-M.; Kovarik, L.; Stach, E. A.; Wang, L.-L.; Salmeron, M.; Somorjai, G. A.; Zheng, H. Revealing the Atomic Restructuring of Pt–Co Nanoparticles. Nano Lett. 2014, 14, 3203–3207.
- (34) Chung, D. Y.; Jun, S. W.; Yoo, G.; Kwon, S. G.; Shin, D. Y.; Seo, P.; Yoo, J. M.; Shin, H.; Chung, Y.-H.; Kim, H.; Mun, B. S.; Lee, K.-S.; Lee, N.-S.; Yoo, S. J.; Lim, D.-H.; Kang, K.; Sung, Y.-E.; Hyeon, T. Highly Durable and Active PtFe Nanocatalyst for Electrochemical Oxygen Reduction Reaction. *J. Am. Chem. Soc.* **2015**, 137, 15478–15485.

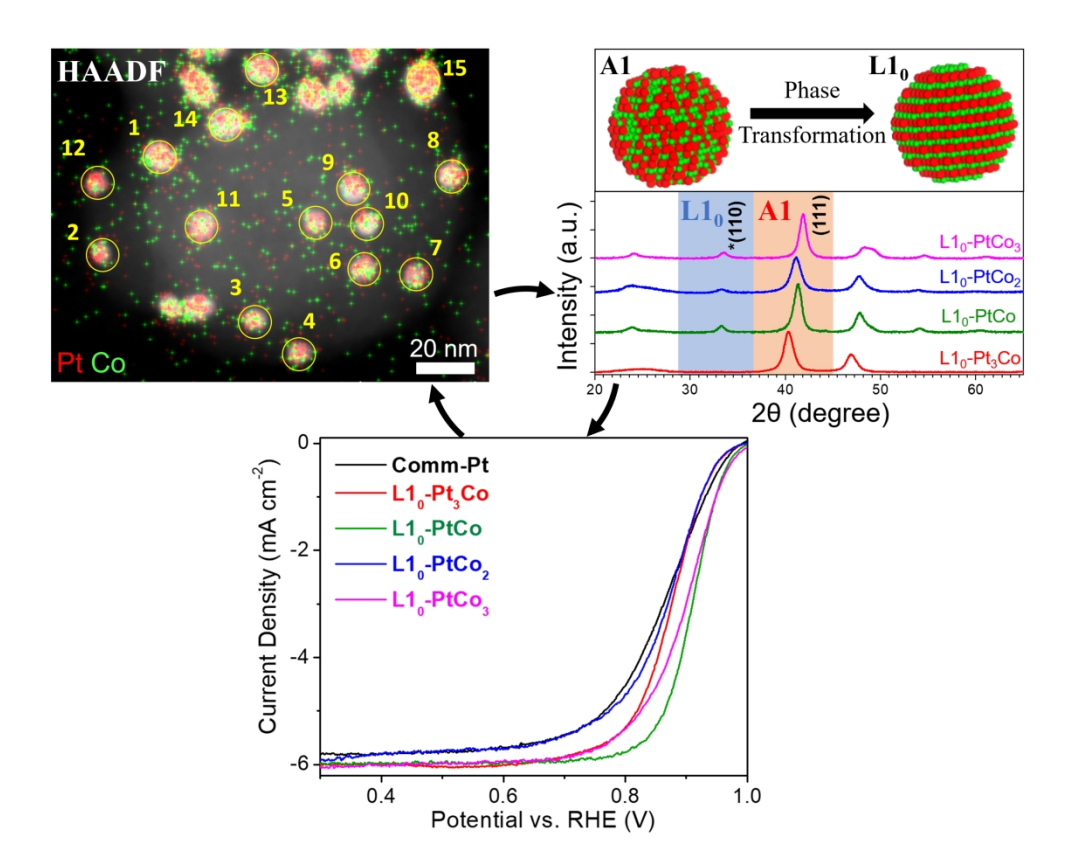
- (35) Xiao, W.; Lei, W.; Gong, M.; Xin, H. L.; Wang, D. Recent Advances of Structurally Ordered Intermetallic Nanoparticles for Electrocatalysis. *ACS Catal.* **2018**, 8, 3237–3256.
- (36) Li, J.; Sharma, S.; Liu, X.; Pan, Y.-T.; Spendelow, J. S.; Chi, M.; Jia, Y.; Zhang, P.; Cullen, D. A.; Xi, Z.; Lin, H.; Yin, Z.; Shen, B.; Muzzio, M.; Yu, C.; Kim, Y. S.; Peterson, A. A.; More, K. L.; Zhu, H.; Sun, S. Hard-Magnet L1₀-CoPt Nanoparticles Advance Fuel Cell Catalysis. *Joule* **2019**, 3, 1–12.
- (37) Li, J.; Xi, Z.; Pan, Y.-T.; Spendelow, J. S.; Duchesne, P. N.; Su, D.; Li, Q.; Yu, C.; Yin, Z.; Shen, B.; Kim, Y. S.; Zhang, P.; Sun, S. Fe Stabilization by Intermetallic L1₀-FePt and Pt Catalysis Enhancement in L1₀-FePt/Pt Nanoparticles for Efficient Oxygen Reduction Reaction in Fuel Cells. *J. Am. Chem. Soc.* **2018**, 140, 2926–2932.
- (38) Sun, S.; Murray, C.B.; Weller, D.; Folks, L.; Moser, A. Monodisperse FePt Nanoparticles and Ferromagnetic FePt Nanocrystal Superlattices. *Science* **2000**, 287, 1989–1992.
- (39) Ristau, R. A.; Barmak, K.; Lewis, L. H.; Coffey, K. R.; Howard, J. K. On the Relationship of High Coercivity and L1₀ Ordered Phase in CoPt and FePt Thin Films. *J. Appl. Phys.* **2012**, 86, 4527–4533.
- (40) Bu, L.; Guo, S.; Zhang, X.; Shen, X.; Su, D.; Lu, G.; Zhu, X.; Yao, J.; Guo, J.; Huang, X. Surface Engineering of Hierarchical Platinum-Cobalt Nanowires for Efficient Electrocatalysis. *Nat. Commun.* **2016**, 7, 1–10.
- (41) Jung, W. S.; Popov, B. N. New Method to Synthesize Highly Active and Durable Chemically Ordered Fct-PtCo Cathode Catalyst for PEMFCs. *ACS Appl. Mater. Interfaces* **2017**, 9, 23679–23686.

- (42) Zhao, Y.; Liu, J.; Zhao, Y.; Wang, F. Composition-Controlled Synthesis of Carbon-Supported Pt–Co Alloy Nanoparticles and the Origin of Their ORR Activity Enhancement. *Phys. Chem. Chem. Phys.* **2014**, 16, 19298–19306.
- (43) Koh, S.; Yu, C.; Mani, P.; Srivastava, R.; Strasser, P. Activity of Ordered and Disordered Pt-Co Alloy Phases for the Electroreduction of Oxygen in Catalysts with Multiple Coexisting Phases. *J. Power Sources* **2007**, 172, 50–56.
- (44) Koh, S.; Toney, M. F.; Strasser, P. Activity–Stability Relationships of Ordered and Disordered Alloy Phases of Pt₃Co Electrocatalysts for the Oxygen Reduction Reaction (ORR). *Electrochim. Acta* **2007**, 52, 2765–2774.
- (45) Shevchenko, E. V.; Talapin, D. V.; Rogach, A. L.; Kornowski, A.; Haase, M.; Weller, H. Colloidal Synthesis and Self-Assembly of CoPt₃ Nanocrystals. *J. Am. Chem. Soc.* **2002**, 124, 11480–11485.
- (46) Heiney, P. A. Datasqueeze: A Software Tool for Powder and Small-Angle X-Ray Diffraction Analysis. *Comm. Powder Diffr. Newsl.* **2005**, 32, 9–11.
- (47) Gordon, T. R.; Diroll, B. T.; Paik, T.; Doan-Nguyen, V. V. T.; Gaulding, E. A.; Murray,
 C. B. Characterization of Shape and Monodispersity of Anisotropic Nanocrystals through
 Atomistic X-Ray Scattering Simulation. *Chem. Mater.* 2015, 27, 2502–2506.
- (48) Luo, J.; Lee, J. D.; Yun, H.; Wang, C.; Monai, M.; Murray, C. B.; Fornasiero, P.; Gorte, R. J. Base Metal-Pt Alloys: A General Route to High Selectivity and Stability in the Production of Biofuels from HMF. *Appl. Catal.*, *B* **2016**, 199, 439–446.

- (49) Alloyeau, D.; Ricolleau, C.; Mottet, C.; Oikawa, T.; Langlois, C.; Le Bouar, Y.; Braidy, N.; Loiseau, A. Size and Shape Effects on the Order-Disorder Phase Transition in CoPt Nanoparticles. *Nat. Mater.* **2009**, 8, 940–946.
- (50) Han, B.; Carlton, C. E.; Kongkanand, A.; Kukreja, R. S.; Theobald, B. R.; Gan, L.; O'Malley, R.; Strasser, P.; Wagner, F. T.; Shao-Horn, Y. Record Activity and Stability of Dealloyed Bimetallic Catalysts for Proton Exchange Membrane Fuel Cells. *Energy Environ. Sci.* **2015**, 8, 258–266
- (51) Gan, L.; Heggen, M.; O'Malley, R.; Theobald, B.; Strasser, P. Understanding and Controlling Nanoporosity Formation for Improving the Stability of Bimetallic Fuel Cell Catalysts. *Nano Lett.* **2013**, 13, 1131–1138.
- (52) Takahashi, Y. K.; Koyama, T.; Ohnuma, M.; Ohkubo, T.; Hono, K. Size Dependence of Ordering in FePt Nanoparticles. *J. Appl. Phys.* **2004**, 95, 2690–2696.
- (53) Yokota, T.; Gao, L.; Zhang, R.; Nicholl, L.; Yan, M. L.; Sellmyer, D. J.; Liou, S. H. The Perpendicular Magnetic Anisotropy of CoPt/Au Multilayer Films. *J. Magn. Magn. Mater.* **2005**, 286, 301–305.
- (54) Franke, P.; Neuschütz, D. Co–Pt, in Binary systems. Part 2: Elements and Binary Systems from B C to Cr Zr: Phase Diagrams, Phase Transition Data, Integral and Partial Quantities of Alloys; Franke, P., Neuschütz, D., Eds.; Springer: Berlin, Heidelberg, 2004; pp 1–4.
- (55) Zeng, H.; Sun, S.; Sandstrom, R. L.; Murray, C. B. Chemical Ordering of FePt Nanoparticle Self-Assemblies by Rapid Thermal Annealing. *J. Magn. Magn. Mater.* **2003**, 266, 227–232.

- (56) Cullity, B. D.; Graham, C. D. *Introduction to the Magnetic Materials*, 2nd ed.; John Wiley & Sons: NJ, 2009; pp 218–221.
- (57) Weller, D.; Moser, A.; Folks, L.; Best, M. E.; Lee, W.; Toney, M. F.; Schwickert, M.; Thiele, J.-U.; Doerner, M. F. High Ku Materials Approach to 100 Gbits/in². *IEEE Trans. Magn.* **2000,** 36, 10–15.
- (58) Schmidt, T. J.; Gasteiger, H. A.; Stäb, G. D.; Urban, P. M.; Kolb, D. M.; Behm, R. J. Characterization of High-Surface-Area Electrocatalysts Using a Rotating Disk Electrode Configuration. *J. Electrochem. Soc.* **1998**, 145, 2354–2358.
- (59) Wang, D.; Yu, Y.; Xing, H. L.; Hovden, R.; Ercius, P.; Mundy, J. A.; Chen, H.; Richard, J. H.; Muller, D. A.; Disalvo, F. J.; Abruña, H. D. Tuning Oxygen Reduction Reaction Activity via Controllable Dealloying: A Model Study of Ordered Cu₃Pt/C Intermetallic Nanocatalysts. *Nano Lett.* **2012**, 12, 5230–5238.
- (60) Allen J. Bard, L. R. F. *Electrochemical Methods: Fundamentals and Applications*, 2nd ed.; Wiley & Sons: NY, 2000.
- (61) Schulenburg, H.; Müller, E.; Khelashvili, G.; Roser, T.; Bönnemann, H.; Wokaun, A.; Scherer, G. G. Heat-Treated PtCo₃ Nanoparticles as Oxygen Reduction Catalysts. *J. Phys. Chem. C* **2009**, 113, 4069–4077.
- (62) Wang, C.; Wang, G.; van der Vliet, D.; Chang, K. C.; Markovic, N. M.; Stamenkovic, V. R. Monodisperse Pt₃Co Nanoparticles as Electrocatalyst: The Effects of Particle Size and Pretreatment on Electrocatalytic Reduction of Oxygen. *Phys. Chem. Chem. Phys.* **2010**, 12, 6933–6939.

- (63) Gan, L.; Rudi, S.; Cui, C.; Heggen, M.; Strasser, P. Size-Controlled Synthesis of Sub-10 nm PtNi₃ Alloy Nanoparticles and Their Unusual Volcano-Shaped Size Effect on ORR Electrocatalysis. *Small* **2016**, 12, 3189–3196.
- (64) Koh, S.; Leisch, J.; Toney, M. F.; Strasser, P. Structure-Activity-Stability Relationships of Pt–Co Alloy Electrocatalysts in Gas-Diffusion Electrode Layers. *J. Phys. Chem. C* **2007**, 111, 3744–3752.



270x215mm (300 x 300 DPI)